Quaternary Science Reviews 195 (2018) 109–121

Contents lists available at ScienceDirect

Quaternary Science Reviews

journal homepage: www.elsevier.com/locate/quascirev

Assessing tectonic and climatic controls for Late Quaternary fluvial terraces in Guide, Jianzha, and Xunhua Basins along the Yellow River on the northeastern Tibetan Plateau

Xiaohua Guo [a, b], Steven L. Forman [a, *], Liliana Marin [a], Xiaolin Li [c]

[a] Department of Geosciences, Baylor University, One Bear Place #97354, Waco, TX, 76798, USA
[b] Shandong Provincial Key Laboratory of Depositional Mineralization & Sedimentary Mineral, Shandong University of Science and Technology, China
[c] Key Laboratory of Environmental Geology of Qinghai Province, Qinghai Province 906, Qinghai Institute of Geological Investigation, 81008, Xining, China

ARTICLE INFO

Article history:
Received 19 February 2018
Received in revised form
21 June 2018
Accepted 4 July 2018
Available online 18 July 2018

Keywords:
Tibetan Plateau
Terraces
Fluvial incision
Landslide dams
Lacustrine sediments
OSL dating

ABSTRACT

This study focused on well-preserved fluvial terrace sequences that span the past 100 ka in the Guide, Jianzha, and Xunhua basins along the Yellow River that drained the northeastern Tibetan Plateau. New geomorphic, stratigraphic, sedimentologic and chronologic data from twelve depositional sequences within terraces yielded better constraints on rates of incision, degradational and aggradational phases for the Yellow River. Age control was established by sixteen OSL ages on quartz grains from fluvial sediments. Three fluvial aggradational phases were identified between 100 and 80 ka, 53 and 40 ka and 21 and 12 ka associated with terrace levels respectively at 120 to 95, 61 to 45 and 25 to 15 m above river level. These aggradational phases reflect multiple processes including enhanced fluvial discharge, sediment availability with glaciation, deglaciation and increased monsoonal precipitation. The initiation of fluvial degradation was linked to mega-floods released from landslide-dammed lakes at ca. 76, 38, and 16 ka, though these changes may also reflect variations in sediment-load discharge relations with climate change. The apparent net incision rate is 1.13 ± 0.11 mm/yr for the past 100 ka and is consistent with late Cenozoic tectonic uplift rates >0.5–2 mm/yr and recent GPS-based rates. The fluvial dynamics of the upper reach of the Yellow River was variably controlled by climate-induced changes in discharge sediment-load relations on stadial to interstadial timescales, episodic mega-floods from the breach of landslide dams, and with net incision in the past 100 ka in response to tectonic uplift of the Tibetan Plateau.

© 2018 Elsevier Ltd. All rights reserved.

1. Introduction

The past hydrodynamic states of the Yellow River, which spans much of the breadth of China, reflect complex interactions amongst allogeneic factors such as sea level, tectonics, and climate change and autogenic forces including lithology, fluvial dynamics, and flooding (Vandenberghe, 2003; Limaye and Lamb, 2016). Fluvial stratigraphic sequences and associated loess deposits for terraces have provided valuable insights on aggradational and degradational history of the Yellow River within the context of late Cenozoic uplift of the Tibetan Plateau (Li, 1991; Li et al., 1996, 1997; Harkins et al., 2007; Pan et al., 2009; Wang et al., 2010; Hu et al., 2016). The formation of the Yellow River drainage along the margin of the Tibetan Plateau, near Lanzhou initiated about 1.8 Ma with fluvial incision propagating steadily westward for the Late Pleistocene (Fig. 1) (Li et al., 1997; Fang et al., 2005; Craddock et al., 2010). This incision appears to be in response to a cooling climate with expansion of lakes across the eastern Tibetan Plateau, spillover, erosion and drainage integration, leading to the entrenchment of the Yellow River (Craddock et al., 2010). The Yellow River incised into Guide Basin ca. 1.7 Ma (Fang et al., 2005) and deeply into the Jianzha Basin (Fig. 1) ca. 1.1 Ma (Pan et al., 1996). Fluvial degradation formed the 700–900 m deep Jishi and Longyang bedrock gorges (Fig. 1) at least by 1.1 and 0.125 Ma, respectively. Initial incision in the Tongde Basin, ~100 km to the south of Gonghe Basin, was apparently recent at ca. 0.5 Ma based on ^{10}Be and ^{26}Al burial ages for quartz-rich fluvial sands, possibly reflecting local base-level controlled by a bedrock sill (Craddock et al., 2010). The

* Corresponding author.
E-mail address: Steven_Forman@Baylor.edu (S.L. Forman).

https://doi.org/10.1016/j.quascirev.2018.07.005
0277-3791/© 2018 Elsevier Ltd. All rights reserved.

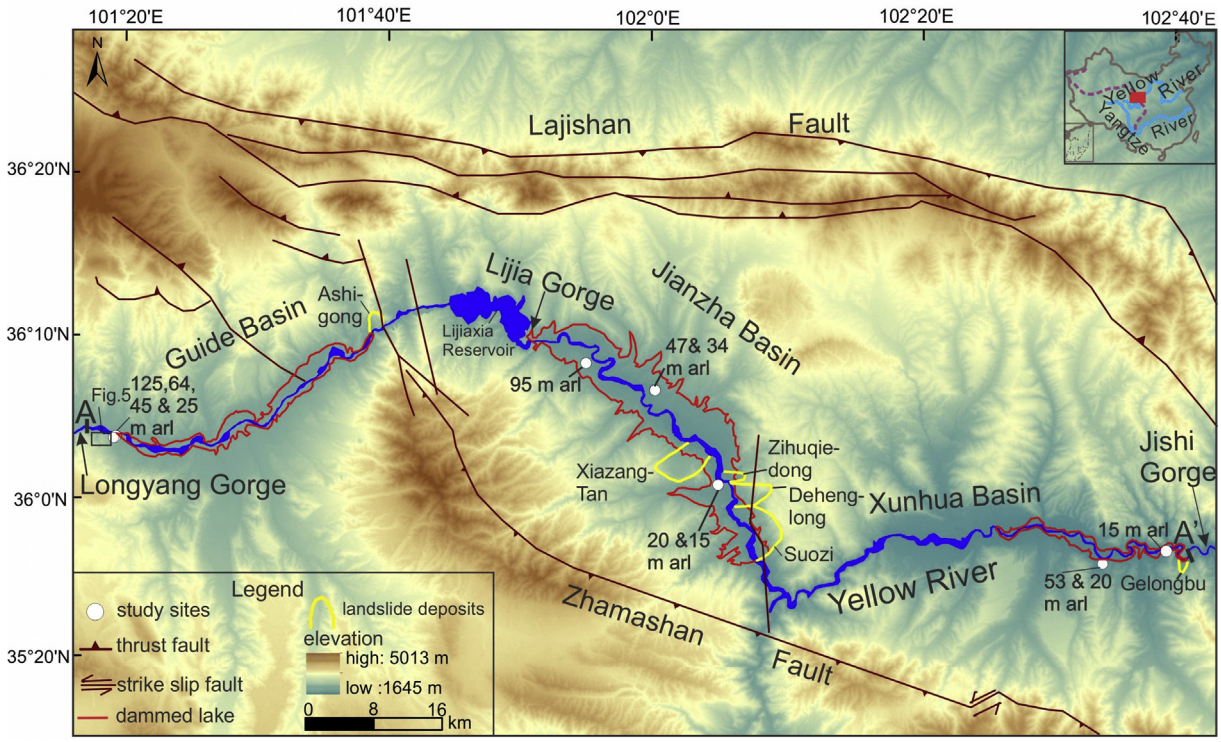

Fig. 1. Location of terraces, landslides and extent of landslide-dammed lakes along the Yellow River for the Guide, Jianzhua and Xunhua basins. Faults system shown is from the Qinghai Geological Survey (1971), Zhang et al. (2007) and Li et al. (2013).

latest period of incision in the Gonghe Basin occurred soon after ca. 0.5 Ma, based on ^{10}Be and ^{26}Al burial ages for quartz-rich fluvial sands from the highest terrace at the Daotanghe Divide (Zhang et al., 2014).

Fluvial terraces along the Yellow River are conspicuous and form a sequence of at least twelve elevationally-distinct levels spanning the middle to the late Quaternary (Li et al., 1997; Zhao and Liu, 2003; Pan et al., 2009; Zhang et al., 2009; Wang et al., 2010; Guo et al., 2012; Hu et al., 2017). These terraces have been identified by enumeration (T1, T2, T3 etc.) from the lowest to the highest elevation and were often dated by the overlying stratigraphic succession of loess units and paleosols (Li et al., 1997; Zhao and Liu, 2003; Pan et al., 2009; Hu et al., 2017). Nine conspicuous terraces (T1-T9) were identified in the Guide Basin that occurred from ~5 to 220 meters above the current river level (m arl) (Zhao and Liu, 2003). The age of the nine terraces was constrained by thermoluminescence (TL) ages on quartz grains from overbank deposits for the lowest (T1) to the highest (T9) terraces at ca. 9, 18, 43, 53, 88, 105, 140, 187 and > 187 ka (Zhao and Liu, 2003). Subsequently, electron spin resonance dating of quartz grains yielded respective mean ages for T1, T2, T4 and T5 of ca. 8, 16, 40 and 81 ka, consistent with the TL ages, though errors in the ages are 10–20% (Miao et al., 2012).

The formation of depositional terraces along the Yellow River is often associated with a prolonged period of lateral accretion and aggradation followed by incision forming the terrace scarp. The processes of aggradation and incision may be variable spatially and temporally with significant lateral planation, erosion, truncation and cut and fill depositional sequences. Landslides in mountainous, tectonically-active areas, like the upper reaches of the Yellow River are important factors for the fluvial evolution of this large river system (e.g. Korup and Montgomery, 2008; Egholm et al., 2013; Croissant et al., 2017). The associated damming effect of landslides and subsequent rapid release of impounded water has immediate and lasting effects on fluvial dynamics and can trigger net aggradation, lateral erosion, channel narrowing and rapid incision (e.g. Korup et al., 2010; Croissant et al., 2017). Thus, rapid down-cutting of some reaches of the Yellow River may have been paced by mega-floods with discharge on the order of 10^6–10^7 m^3/s derived from breaches of landslide-dammed lakes at ca. 76, 38, 24 and 16 ka (Ma et al., 2014; Yin, 2014; Guo et al., 2016; Wu et al., 2016). Recent results from a two-dimensional hydro-sedimentary model indicated that about 50% of the coarse-sediment volume of a large landslide is eroded in 5–25 years post landslide emplacement which resulted in a breach of the dammed lake with a mega-flood release (Croissant et al., 2017).

The preservation of terrace sequences along the Yellow River indicates a persistent process to lower base level on 10^4 year timescales to facilitate net fluvial incision, within the context of Pleistocene climate variability (e.g. Church and Ryder, 1972; Hancock and Anderson, 2002; Bridgland and Westaway, 2008a). Base level lowering in continental interiors can reflect differential uplift with tectonic activity, isostatic response to denudation, and from far-field vertical motion associated with subduction, faulting, and deformation of strata (Westaway et al., 2003; Westaway and Bridgland, 2014; Bridgland et al., 2017). In the absence of these mechanisms, reoccupation of terrace treads by a fluvial system may erode the geomorphic and stratigraphic records of fluvial processes. Model simulations of terrace formation suggested that the preservation of multiple terraces can be influenced by uplift rates. These simulations indicate that interpreting terrace records may be difficult in regions where climate variations were superimposed on spatial and temporal variations in tectonically-driven uplift. Uplift rates for the eastern Tibetan Plateau during the late Cenozoic are between 0.5 and 2 mm/year (Clark et al., 2005; Deng et al., 2013; Zhang and Jin, 2013; Pan et al., 2016) which serve to isolate elevationally terrace sequences above flood erosion on 10^4-year timescales. Thus, the terrace sequence of the Yellow River provides

an important archive to assess the relative roles of climate change, autogenic processes, and regional uplift on fluvial morphodynamics in the late Quaternary.

Uncertainty remains on the timing of fluvial terrace formation and abandonment with climatic oscillations in the late Quaternary, as reflected in glaciation and deglaciation of the Tibetan Plateau. Terrace formation *sensu lato* may correlate broadly with glacial advances (Molnar et al., 1994; Nivière et al., 2016; Limaye and Lamb, 2016), with the onset of deglaciation (Bull, 1990; Pan et al., 2009; He et al., 2015) and with glacial to interstadial transitions (Antoine et al., 2000; Cordier et al., 2017). Often terrace formation was contextualized as reflecting cyclic climate variability with insolation variability, such that river downcutting occurred primarily at warming or cooling transitions (Bridgland, 2000; Bridgland and Westaway, 2008a, 2008b; Vandenberghe, 2008).

An enduring challenge to better understand the complex drivers and variable response of fluvial systems is the paucity of well-dated terrace records spanning the past 100 ka. This study focused on the sedimentologic record and associated OSL chronology for the lower six depositional terraces along the upper reaches of the Yellow River. This new data is pertinent to address the effect of tectonics, the impact of large floods from landslide-dammed lakes, and the timing of glaciation and deglaciation of the Tibetan Plateau upon terrace formation and the degradation of the Yellow River in the Late Pleistocene.

2. Sedimentologic and tectonic context

The Yellow River, one of the largest rivers in the world, originates in the northeast Qinghai-Tibetan Plateau with an average altitude of ~4000 m. This river descends through the Cenozoic Guide, Jianzha and Xunhua basins (Fig. 1) with an average elevation of ~2205 m (Fig. 1). These three 30-km wide basins trend northwest-southeast and are separated by intervening bedrock sills forming the Longyang, Lijia, and Jishi gorges (Fig. 1). There are many thrust faults that cross the Yellow River (Fig. 1). The Lajishan thrust fault which fronts the Lajishan Mountain (Fig. 1) was active in the Late Pleistocene (Qinghai Earthquake Administration, 1989). The common occurrence of landslides in the study area may reflect earthquake events from nearby active thrust faults and some of these landslides have resulted in damming of the Yellow River in the late Quaternary (Ma et al., 2014; Yin, 2014; Guo et al., 2016; Wu et al., 2016).

The late Quaternary fluvial dynamics of the Yellow River was assessed by stratigraphic assessment and associated sixteen new OSL ages (Table 1) for twelve stratigraphic sections through depositional terraces of the various basins (Fig. 2). The OSL dating of quartz grains from fluvial sediments provided age estimates for aggradation, maximum limiting ages for subsequent degradation, and timing for formation of terraces. The terraces were depositional in origin and in places deposited on or into Neogene red mudstone or Eocene brick-red sandstone.

The sedimentology of terrace deposits was well exposed in a series excavations or natural exposures (Fig. 2). Fluvial aggradational sequences were recognized stratigraphically as crudely stratified basal gravels, transitioning to stratified gravelly-sands, and capped by massive to stratified silts and fine sand. A recognized depositional facies was of a point or channel bar characterized by a fining upwards sequence. Often low-angle cross beds occurred with centimeter-scale laminations composed of moderately sorted, coarse to fine sand, with scattered 5-to-10 cm diameter rounded pebbles and intercalated with decimeter-thick lenses of better sorted medium to coarse sand (Fig. 3a and Fig. 3b). The overbank sediments were typically a silty, very-fine sand to a medium sand with centimeter to millimeter scale, near-horizontal bedding (Fig. 3a). Above the overbank sediment there was often a paleosol/loess complex (Fig. 3a). The paleosols exhibited a brownish color and pedogenic features, such as disseminated organic matter, subangular blocky structure, translocated clay, orange iron-oxide coatings, and in some places carbonate filaments or nodules (Fig. 3a) (Guo et al., 1991). The grayish-yellow, silt-loam, massive loess are characteristic of deposits within the catchment of

Table 1
OSL ages on quartz extracts and associated data for fluvial sediments for Guide, Jianzha and Xunhua basins, Yellow River, China.

	Sample height/terrace elevation	Sample	Lab	Grain size		D_e	Over-dispersion	U	Th	K	Cosmic dose	Dose rate	OSL age
	(m)	ID	number	Aliquots	(μm)	(Gray)[a]	(%)[b]	(ppm)[c]	(ppm)[c]	(%)[c]	(mGray/yr)[d]	(mGray/yr)[e]	(ka)[f]
Guide	25/27	NN2-1	BG4181	35/35	63–100	60.11 ± 4.06	16 ± 2	2.75 ± 0.01	11.25 ± 0.01	1.86 ± 0.01	0.29 ± 0.029	3.07 ± 0.01	19.5 ± 1.6
	25/27	NN2-2	BG4182	35/35	63–100	65.12 ± 4.22	13 ± 1	2.83 ± 0.01	12.05 ± 0.01	1.58 ± 0.01	0.29 ± 0.029	3.14 ± 0.01	20.7 ± 1.7
	24/27	NN2-3	BG4183	32/35	63–100	75.11 ± 2.70	19 ± 2	2.98 ± 0.01	10.50 ± 0.01	2.21 ± 0.01	0.26 ± 0.026	3.65 ± 0.01	20.5 ± 1.4
	45/51	NN3-1	BG4184	30/35	150–250	108.52 ± 6.39	22 ± 3	1.40 ± 0.01	7.76 ± 0.01	2.07 ± 0.01	0.18 ± 0.018	2.73 ± 0.01	39.7 ± 3.4
	64/67	NN4-1	BG4193	33/35	100–150	100.19 ± 3.64	21 ± 2	2.07 ± 0.01	10.9 ± 0.01	2.12 ± 0.01	0.28 ± 0.01	3.27 ± 0.01	30.6 ± 2.4
	125/126	NN5-1	BG4194	34/35	150–250	89.79 ± 6.62	23 ± 2	1.90 ± 0.01	7.85 ± 0.01	1.54 ± 0.01	0.29 ± 0.01	2.37 ± 0.01	37.8 ± 3.8
Jianzha	15/30	JZ3-1	BG4104	30/35	100–150	45.73 ± 2.33	24 ± 3	2.60 ± 0.01	9.17 ± 0.01	1.54 ± 0.01	0.12 ± 0.012	2.70 ± 0.01	16.9 ± 1.3
	16/20	JZ2-1	BG4090	40/50	100–150	34.19 ± 1.42	24 ± 2	1.33 ± 0.01	5.76 ± 0.01	2.24 ± 0.01	0.17 ± 0.017	2.95 ± 0.01	11.5 ± 0.9
	20/26	JZ2-2	BG4089	37/50	100–150	46.85 ± 2.00	24 ± 3	1.79 ± 0.01	5.98 ± 0.01	1.96 ± 0.01	0.19 ± 0.019	2.65 ± 0.01	17.6 ± 1.3
	34/39	JZ4-1	BG4105	26/57	150–250	54.48 ± 3.92	20 ± 3	1.30 ± 0.01	5.34 ± 0.01	1.66 ± 0.01	0.13 ± 0.013	2.15 ± 0.01	25.3 ± 2.4
	47/57	JZ5-3	BG4123	30/35	100–150	108.92 ± 5.00	21 ± 3	2.48 ± 0.01	9.64 ± 0.01	1.89 ± 0.01	0.12 ± 0.012	2.37 ± 0.13	45.9 ± 3.5
	47/57	JZ5-1	BG4122	34/35	150–250	182.32 ± 8.93	21 ± 2	1.64 ± 0.01	8.05 ± 0.01	2.11 ± 0.01	0.11 ± 0.011	2.77 ± 0.11	65.8 ± 5.2
Xunhua	15/27	XH2-2	BG4177	35/35	63–100	47.45 ± 1.68	10 ± 1	2.37 ± 0.01	9.15 ± 0.01	1.89 ± 0.01	0.08 ± 0.008	2.92 ± 0.01	16.2 ± 1.1
	20/23	XH4-1	BG4156	40/46	63–44	54.16 ± 1.79	19 ± 2	2.62 ± 0.01	10.15 ± 0.01	2.00 ± 0.01	0.02 ± 0.002	3.14 ± 0.01	17.2 ± 1.2
	20/23	XH4-2	BG4157	33/35	63–44	56.67 ± 3.44	14 ± 3	1.94 ± 0.01	7.55 ± 0.01	2.10 ± 0.01	0.20 ± 0.020	3.06 ± 0.01	18.5 ± 1.6
	67/76	XH5-3	BG4178	34/35	150–250	141.81 ± 6.02	20 ± 2	1.53 ± 0.01	6.21 ± 0.01	2.43 ± 0.01	0.27 ± 0.027	3.04 ± 0.01	46.6 ± 3.8

[a]Aliquot number used for SAR. Equivalent dose calculated using the central age model of Galbraith and Roberts (2012).
[b]Equivalent dose (D_e) analyzed under blue-light excitation (470 ± 20 nm) by single aliquot regeneration protocols (Murray and Wintle, 2003; Wintle and Murray, 2006).
[c]Values reflect precision beyond instrumental errors; values of ≤25 indicate low dispersion in equivalent dose values with a log normal distribution (Galbraith and Roberts, 2012).
[d]U, Th and K_2O content analyzed by inductively coupled plasma-mass spectrometry (ICP-MS) analyzed by ALS Minerals Incorporation, Reno, Nevada, USA.
[e]From Prescott and Hutton (1994). Water content was assumed 10 ± 3 by weight.
[f]Systematic and random errors calculated in a quadrature at one standard deviation. Datum year is AD 2010.

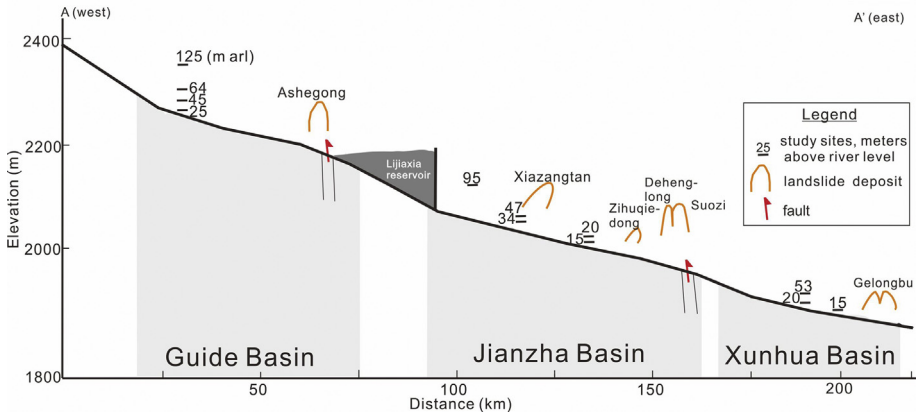

Fig. 2. Longitudinal profile of the upper Yellow River from the Point A to A′ in Fig. 1, with projection of terraces and landslides that blocked the channel (brown arcuate lines). Red lines are active faults. Location indicated in Fig. 1. Profile was extracted from Google Earth, with 3X vertical exaggeration. (For interpretation of the references to color in this figure legend, the reader is referred to the Web version of this article.)

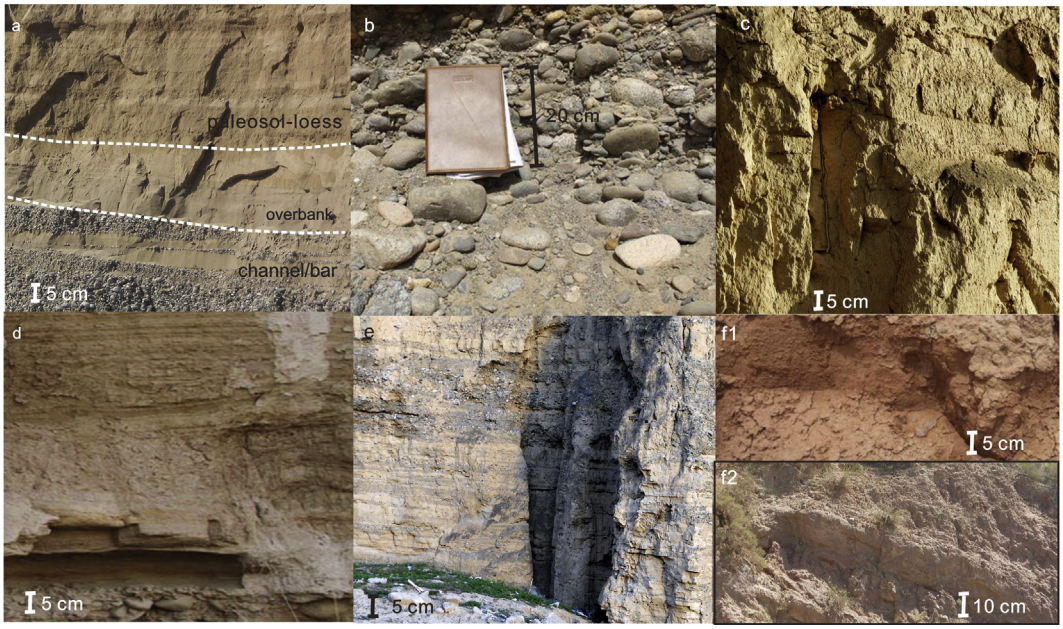

Fig. 3. Photographs of major depositional facies exposed in terrace stratigraphic sections. (a) aggradational sequence with lower strata of pebbly-sand channel/bar deposit, capped by overbank sediments with an uppermost paleosol and loess complex; (b) channel gravel; (c) loess; (d) deep water lake sediment; (e) lake margin sediment; (f1) Neogene red mudstone; (f2) Eocene brick-red sandstone. (For interpretation of the references to color in this figure legend, the reader is referred to the Web version of this article.)

the Yellow River (Liu, 1985) (Fig. 3c).

Lacustrine deposits commonly bury terrace treads at or below 35 m arl within Jianzha and Xunhua basins (Fig. 3d). These sediments demarcated the formation of landslide-induced damming of the Yellow River forming large lakes that extended 10s of kilometers up the drainage (Fig. 1). The landslides may have formed post-earthquake events and/or a result of autogenic process, such as toe slope erosion and a high water table (Ma et al., 2014; Yin, 2014; Guo et al., 2016; Wu et al., 2016). The sedimentology of these lake deposits ranges from a horizontally or a subhorizontally laminated silty sand to a fine sand with millimeter-to-centimeter-scale bedding, reflecting deep-lake conditions (>5 m). Often these lake sediments coarsen upwards with interbeds of sandy silty and/or pebbly sand, which indicated a fall in lake level. Lacustrine sequences in places were capped by lower shoreface to littoral sediments of well-sorted, fine to medium sands, with millimeter-scale planar to sub-planar beds that dip broadly toward the valley center (Fig. 3e); and these sediments were associated with regression of a lake upon dam breach. Lastly, alluvial fans commonly obscure terrace treads especially in the piedmont area. The associated deposits were massive or crudely stratified, poorly to moderately sorted coarse to very coarse sands, with abundant subangular pebbles and cobbles, commonly 1–20 cm in diameter, and with interspersed lenses of moderately sorted medium sand associated with intermittent flowing water.

3. OSL dating

A long-standing concern for the accurate luminescence dating of fluvial sediments has been the possibility of incomplete solar resetting reflecting the attenuation of higher energy spectra and reduced light penetration with turbidity in the water column which lowers the efficiency of solar resetting (e.g. Schokker et al., 2005; Rittenour, 2008). Sediments of lower energy depositional environments such as upper point-bar or upper flood plain facies were sampled for OSL dating to maximize the possibility of complete

solar resetting of grains and reflecting similar water levels across the basins.

OSL ages were determined at the Geoluminescence Dating Research Laboratory at Baylor University, Texas, USA. The laboratory is under subdued illumination from indirect light emitted from a sodium vapor bulb. Particle fractions were separated by sieving and magnetic minerals removed by agitation with magnets. The quartz fraction was then isolated by two density separations (2.6 and 2.7 g/cm^3) using the heavy liquid Na-polytungstate. Further purification of the quartz separate was by an 80-minute immersion in HF (Mejdahl and Christiansen, 1994) which also etched the outer 10–20 μm of quartz grains to remove the alpha effected area. Quartz purity was not assumed but verified by petrographic inspection of the quartz separate. Samples that revealed >1% non-quartz minerals within a hundred grains were soaked a second time in HF and re-checked petrographically. Four representative quartz aliquots for each sample were exposed to infrared light to check for feldspathic components and uniformly yielded emissions <300 counts per second, reflecting background counts and thus, a spectrally pure signal from quartz.

Single Aliquot Regeneration (SAR) protocols (Murray and Wintle, 2003) were applied to estimate the equivalent dose of the quartz fraction (Table 1). Up to 57 aliquots were analyzed for each sample (Table 1). Each aliquot was adhered to 1.5–2.0 mm circular area of ~1 cm diameter aluminum disc which is equivalent to about 150–900 quartz grains, dependent on grain size (Table 1). A series of tests were conducted before the application of SAR protocols for samples from Jianzha and Guide basins to estimate the effect of preheating at 180 °C, 200 °C, 220 °C, 240 °C and 260 °C on the regenerative signal as a dose recovery test (Murray and Wintle, 2003). Three aliquots were tested at each temperature to a total of fifteen aliquots and these sediments appear to be preheat insensitive (within ±10%) to recover a known dose (Fig. 4). The first preheat temperature of 200 °C yielded a consistent recovered dose well within 10% of the known dose (Murray and Wintle, 2003). The second (cut heat) was at 160 °C and the final heating was at 260 °C for 40 s to eliminate potentially carryover of signal.

SAR data collection was with an Automated Risø TL/OSL-DA-20 system with blue light excitation (Bøtter et al., 2000) and a calibrated ^{90}Sr/^{90}Y beta source, using Risø standards. All SAR emissions were integrated over the first 0.8 s of stimulation out of 40 s and the background calculated for the last 30-to 40-s interval. The shine down curves showed that OSL signal is dominated by the so-called fast component (Murray and Wintle, 2003), with the OSL emission decreasing by 95% during the first 0.8 s of stimulation (Fig. 5a). The fast ratio for individual aliquots ranged from 50 to 15 indicating a clear dominance of the fast component (Durcan and Duller, 2011). The regeneration growth curves were well fitted using the exponential-linear function (Fig. 5b).

Equivalent dose distributions were log normal and the scatter in the data was quantified with overdispersion values. An overdispersion percentage of an equivalent dose (D_e) distribution is an estimate of the relative standard deviation from a central D_e value (Galbraith et al., 1999; Galbraith and Roberts, 2012). Overdispersion values > 25% may indicate mixing of grains of various ages or partial solar resetting of grains (Galbraith et al., 1999). Quartz aliquots showed a low overdispersion, below the 25% threshold, indicating high internal consistency in D_e values reflecting a single population of grains (Table 1; Fig. 5b). Samples exhibited overdispersion values between 10 and 25% indicating that within analytical errors the luminescence emissions from quartz grains reflect one dominant equivalent dose population with the final equivalent dose calculated using the Central Age Model (Table 1).

The environmental dose rate is a critical measurement for calculating a luminescence age. This value reflects the exposure of quartz grains to ionizing radiation from the decay of the U and Th series, ^{40}K, ^{87}Rb and cosmic sources during the burial period (Table 1). The U, Th, Rb and K concentrations were determined by inductively coupled plasma-mass spectrometry by ALS Minerals Inc. Reno, Nevada, USA (Table 1). The beta and gamma doses were adjusted according to grain diameter to compensate for mass attenuation in the dose rate calculation (Fain et al., 1999). A cosmic dose component was calculated for each sample considering location, elevation, and depth of strata sampled (Prescott and Hutton, 1994) and this value varied between 0.02 and 0.29 mGy (Table 1). Moisture content (by weight) during the burial period was assumed to be 10 ± 3% (cf. Hou et al., 2012), reflecting current water content of these moderately sorted, but well drained sands.

4. Results

4.1. Guide Basin

Previous studies have reported in the Guide Basin up to nine terraces between 8 and 252 m arl (Zhao and Liu, 2003). This study identified fluvial aggradational sequences associated with terraces at approximately 125, 64, 45 and 25 m arl (Fig. 6). The elevation of terrace was assessed by a GPS receiver with a maximum error of 5 m. The stratigraphy of the 125 m arl terrace showed a basal Triassic gneiss capped by 8-m thick coarse fluvial gravel buried by alluvial fan sediments, and buried by 0.2-m thick loess deposit. This alluvial fan deposit was poorly to moderately sorted, with subangular pebbles, 1–2 cm in diameter, with interspersed lenses of moderately-sorted medium sand. Quartz grains from a fine sand len in the alluvial fan deposit yielded an OSL age of 37.8 ± 3.8 ka (BG 4194) and provided a minimum limiting age on the underlying fluvial deposit (Fig. 7) (Table 1). Thus, this aggradational event occurred prior to ca. 38 ka ago.

The terrace at 64 m arl exhibited a similar stratigraphic sequence to the 125 m arl terrace (Fig. 7). Quartz grains from a lens

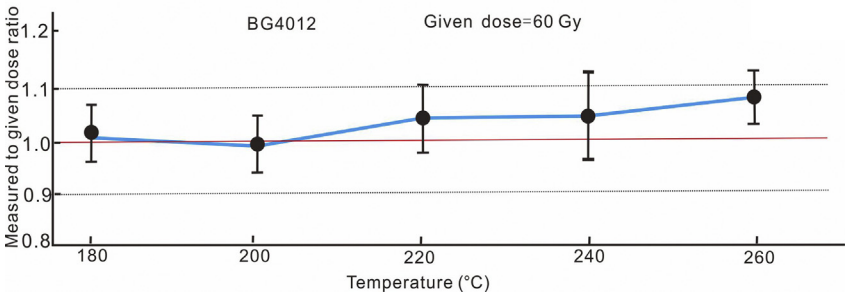

Fig. 4. Dose recovery test for BG4012 for aliquots at temperatures between 180 and 260 °C. These sediments appear to be preheat insensitive (within ±10%) to recover a known dose.

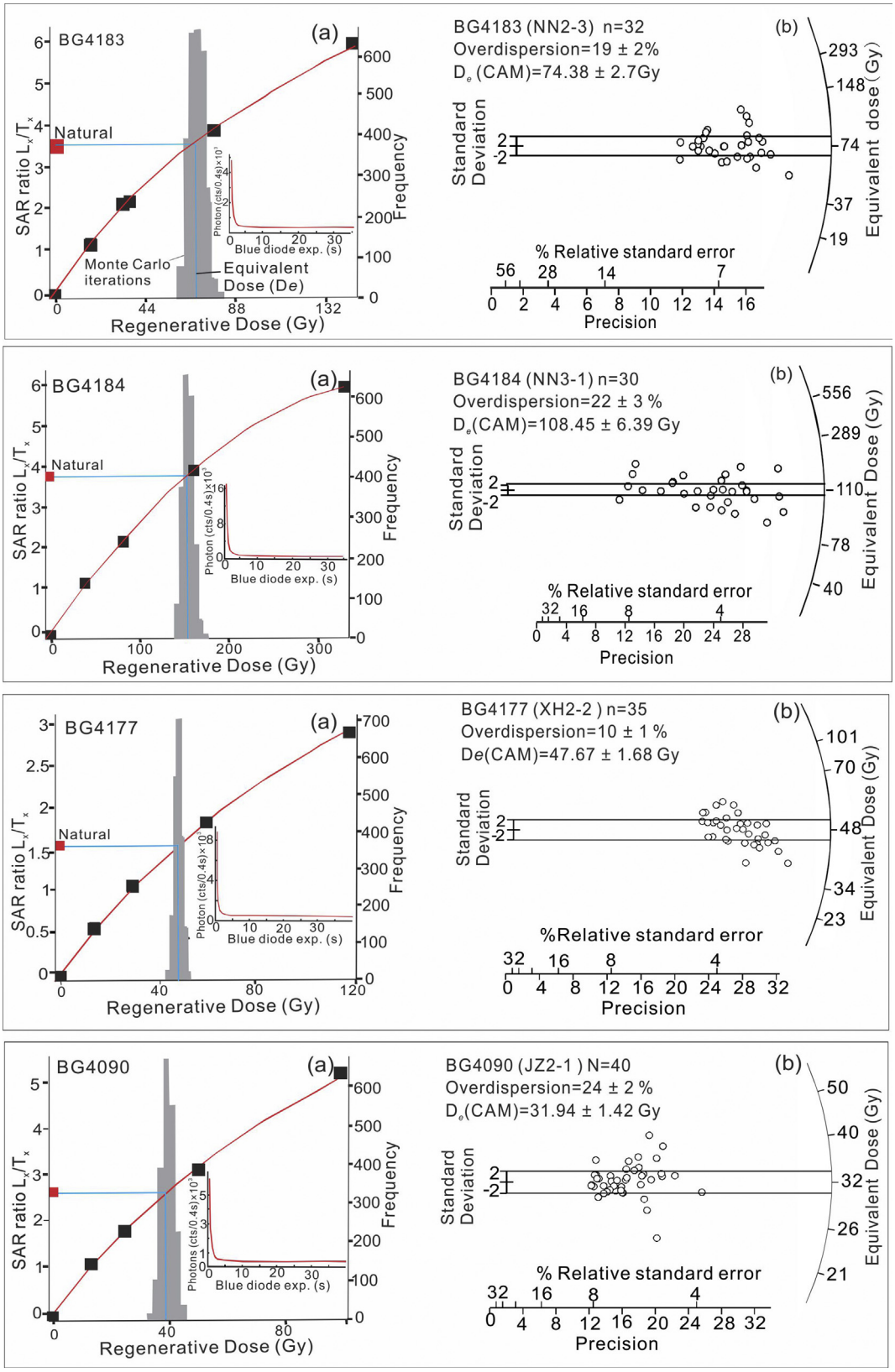

Fig. 5. (a) OSL regenerative growth curves for quartz grains for samples BG4183, BG4184, BG4177 and BG4090 with inset figure showing representative shine-down curve for a natural emission. (b) Radial plots of equivalent dose (D_e) values for aliquots. Shown is the two sigma D_e range for the Central Age Model (CAM) (after Galbraith and Roberts, 2012).

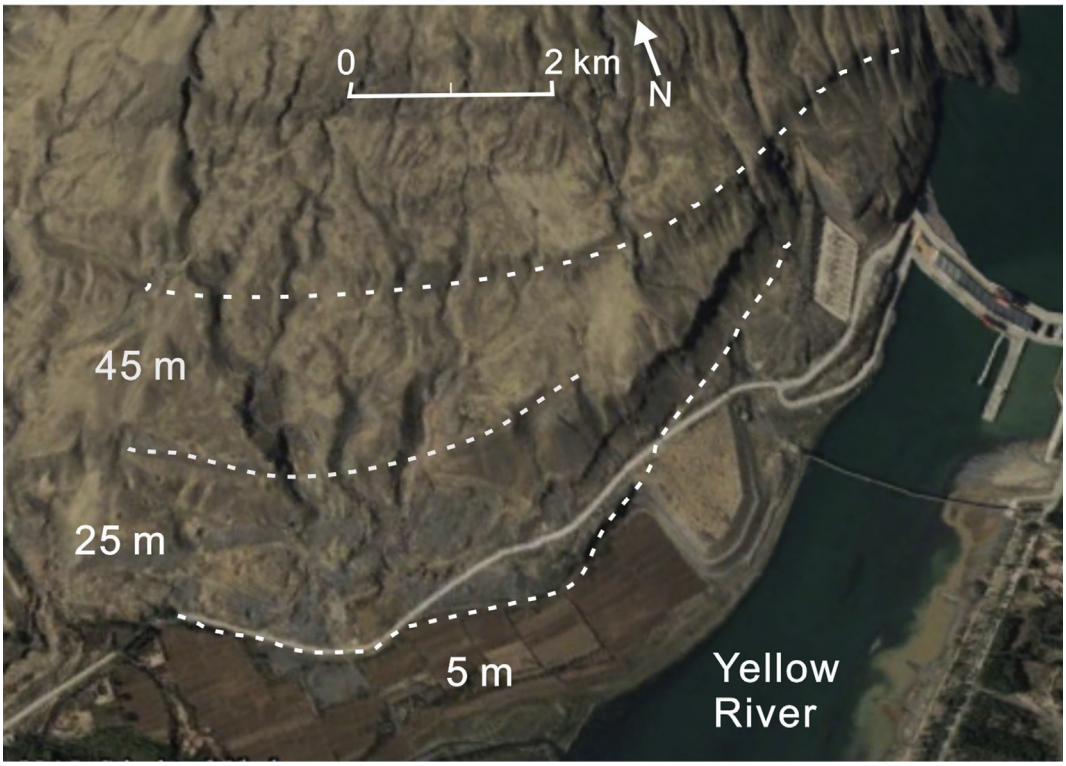

Fig. 6. Photograph showing terraces at 5, 25, and 45 m elevation in the Guide Basin. See Fig. 1 for location.

in the alluvial fan sediments at 64 m arl yielded an OSL age of 30.6 ± 2.4 ka (BG 4193). Thus, fluvial aggradation occurred before 31 ka. Therefore, the ages of terraces at 125 and 64 m arl were constrained by minimum limiting OSL age on overlying alluvial fan sediment, which buried fluvial sediments. Thus, the terraces at 125 and 64 m arl were abandoned before ~40 ka, which is a stratigraphically-consistent minimum-limiting age estimate.

The section in the 45 m arl terrace showed an 8-m thick, cobble-rich gravels overlying Neogene red mudstone and capped by 0.2 m of loess. Quartz grains from a ~40-cm thick sand lens in this gravel unit returned the OSL age of 39.7 ± 3.4 ka (BG 4184) (Table 1) which indicates fluvial aggradation ca. 40 ka ago. This fluvial aggradation may reflect the emplacement of the Ashigong Landslide, 45 km downstream of the 45 m arl section, from inferred earthquake event (s) of the Deqiansi-Ashigong fault system and subsequent landslide impoundment of the Yellow River forming a ~24-km-long lake (Yin, 2014; Guo, 2017). An OSL age on quartz grains of 38.2 ± 2.5 ka from this lake sediment (Guo, 2017) is concordant with fluvial aggradation documented for this 45 m arl terrace site.

A 5-m high section of the terrace at 25 m arl exposed a fluvial aggradational sequence (Fig. 7). The basal sediment was a crudely-bedded gravelly sand, overlain by centimeter-scale, subhorizontally bedded silts and sands with coarser beds of sandy gravels, and capped by loess. OSL ages are stratigraphically consistent at 20.5 ± 1.4 ka (BG 4183) and 20.7 ± 1.7 ka (BG 4182) and 19.5 ± 1.6 ka (BG 4181) on quartz grains (Table 1) from fine sand rich lamina (Fig. 7).

4.2. Jianzha Basin

Little is known about the sedimentology and age of terraces in this basin. River-bank exposures revealed multiple fluvial aggradational sequences for terraces at ~95, 47, 34, 20, and 15 m arl (Fig. 7). The highest terrace at 95 m arl was well exposed along the southern bank of the Yellow River, ~1.5 km down river from the Lijiaxia Reservoir (Fig. 1) and was reported previously by Guo et al. (2016). This terrace section exposed six major stratigraphic units documenting fluvial, lacustrine, and finally loess deposition (Fig. 7). The lowest unit (1) is a 1-m thick gravelly sand capped by unit (2) of well-sorted medium to fine sand, both of fluvial origin. Units 3 and 4 were distinctive, composed of seven meters of centimeter-scale, horizontally bedded lacustrine sandy-silt that conformably overlies a subjacent fluvial sand and gravel. The overlying unit 5 is a matrix-supported gravel-rich diamicton, which is inferred to be a flood deposit, post breach of lake. Quartz grains from a fluvial overbank facies (unit 2) returned an OSL age of 79 ± 6 ka (Guo et al., 2016). The basal lacustrine sediments (unit 4) yield a similar age of 76 ± 8 ka (Guo et al., 2016), and is a close limiting age on emplacement of Dehenglong and Suozi landslides. These contemporary landslides are associated with earthquake activity, about 25 km downstream from this section, that dammed the Yellow River, and formed a lake extending ~46 km up the valley (Guo et al., 2014, 2016) (Fig. 1).

The second to the highest terrace studied at 47 m arl exposed a 15-m thick fluvial sequence with gravelly sand at the base capped by thin eroded loess (Fig. 7). Quartz grains from fine sand lenses interbedded within gravels returned OSL ages of 45.9 ± 3.5 ka (BG 4123) and 65.8 ± 5.2 ka (BG 4122) which suggests two temporally distinct fluvial aggradation events at ca. 66 and 46 ka.

The terrace at 34 m arl showed four stratigraphic units that documented fluvial aggradation followed by formation of a landslide-dammed lake (Fig. 7). The base of the section showed a 3-m thick, well-sorted gravel (unit 1), overlaid by a 0.5-m thick silty-sand overbank deposit (unit 2), and a 7-m thick silty sand interbedded with pebble layers (unit 3), capped by a 1-m thick loess (unit 4; Fig. 7). Unit 2 showed diffuse laminar bedding and was intercalated with a red clay bed, perhaps a flood deposit. The overlying unit 3 was a well-sorted, silty sand intercalated with

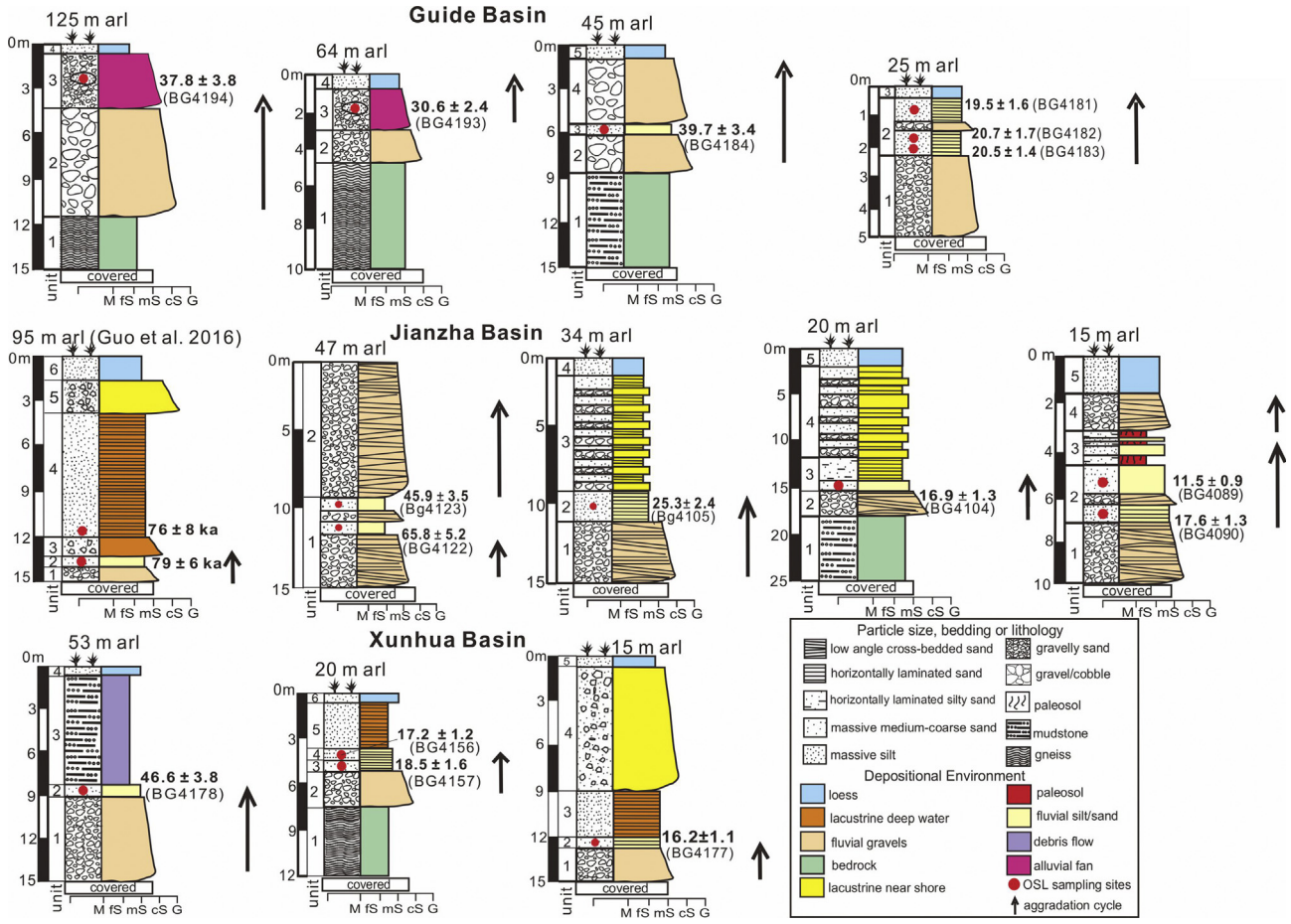

Fig. 7. Stratigraphic sections identified by elevation above the Yellow River (m arl) of highest fluvial deposit within terraces in Guide, Jianzha, and Xunhua basins, showing bedding, particle sized characteristics and associated OSL ages. Section in the Jianzha Basin at 95 m is from (Guo et al., 2016).

sandy, angular pebble-rich beds, indicative of deep to shallow water lacustrine environments, with colluvial input. The overbank silty sand in unit 2 yielded an OSL age of 25.3 ± 2.4 ka (BG 4105), indicating a fluvial aggradation event at ca. 25 ka. This stratigraphic assessment provides a new maximum-limiting age for landslide emplacement of 25.3 ± 2.4 ka (BG 4105) for the underlying fluvial sediments, consistent with a prior ESR age of 24 ± 2 ka on quartz grains below the Xiazangtan landslide, about 8 km downstream from this section (Yin, 2014). The cause of Xiazangtan landslide is unknown, but may reflect landscape instability with strengthened monsoonal precipitation (Zhou, 2011; Guo et al., 2012; Yin, 2014).

The terrace at 20 m arl contained six stratigraphic units that documented fluvial aggradation and the subsequent development of a landslide-dammed lake (Fig. 7). The basal unit was a Neogene red mudstone (unit 1) with a 5-m thick, pebbly-gravel (unit 2) deposited on to this bedrock surface. This clastic sediment transitions up section into a well-sorted medium to coarse sand (unit 3) and reflects fluvial channel and bar deposition. A 9-m thick sequence of interbedded silty and sand beds (unit 4) overlies these fluvial sediments, reflecting subsequent lacustrine deposition. Quartz grains from the basal fluvial sand returned an OSL age of 16.9 ± 1.3 ka (BG 4104) (Table 1). A previous study indicated that the Zihuqiedong Landslide, about 1.5 km down river from this study site, dammed the Yellow River prior to 14.1 ± 1.2 ka based on a single OSL age on the overlying loess (Zhou, 2011). There is now a refined age for this landslide of ca.15 to 16 ka between the new OSL age of 16.9 ka on the subjacent fluvial sand and the previous OSL age of 14.1 ka on overlying loess (Zhou, 2011).

The lowest terrace studied at 15 m arl exposed sediment that indicated prolonged fluvial aggradation interrupted in places by pedogenesis (Fig. 7). The lowest-most aggradational event includes a 3-m thick gravel-rich sand overlain by a 4-m thick, well-sorted medium to fine sand, capped by a paleosol complex developed in overbank silts and sands. The upper most aggradational sequence was demarcated by a fining upward sequence from a 1.5-m thick gravel to 0.6-m thick medium sand deposit (Fig. 7). Quartz grains from bed of fluvial sands yielded OSL ages of 17.6 ± 1.3 ka (BG4089) and 11.5 ± 0.9 ka (BG4090) (Table 1), which suggests repeated occupation of this level by the Yellow River between ca. 18 and 11 ka.

4.3. Xunhua Basin

The highest terraces (>250 m) in Xunhua Basin appear to be > 1 Ma old and serve as a minimum limiting age for incision of the basin (Pan et al., 1996). This study focused on the lower terraces at 53, 20, and 15 m arl, especially those associated with lake sediments deposited post emplacement of a landslide-induced dam (Fig. 7). The basal sediment exposed in the 53 m arl terrace was a 6-m thickness of gravel (unit 1), with an overlying 0.5-m thick overbank silty sand (unit 2). The section was capped by a 5-m thick debris flow deposit composed mostly of red mudstone, derived from local bedrock (unit 3). Quartz grains from the overbank silty sand (unit 2) returned an OSL age of 46.6 ± 3.8 ka (BG4178) which indicates fluvial aggradation ca. 47 ka.

The 20 m arl terrace on the southern bank of the Yellow River

documented fluvial aggradation and formation of a landslide-dammed lake. A section through the terrace at 20 m arl revealed a lower fluvial sequence of a 3-m thick pebbly gravel (unit 2) deposited on to Triassic gneiss (unit 1), overlain by 0.4 m thick, massive, and well-sorted fine sand (unit 3). This section was capped by interbedded fine sand and silty-sand associated with formation of a landslide-dammed lake (units 4 and 5). OSL ages of 18.5 ± 1.6 ka (BG 4157) and 17.2 ± 1.2 ka (BG 4156) on quartz grains from the overbank fine sand (unit 3) indicate fluvial aggradation from ca. 18.5 to 17.2 ka. Emplacement of a landslide and subsequent damming of the drainage occurred soon after 17.2 ka (Fig. 7).

The section through a terrace at 15 m arl, about 5 km down river from the 20 m arl section, revealed considerable thicknesses of fluvial and lacustrine sediments. A 2.5-m thick coarse pebbly-gravel (unit 1) occurs at the section base, overlaid by a 30-cm thick overbank silty sand (unit 2) that transitioned into 3 m thick, horizontally-laminated silty-sand lacustrine sediments (unit 3). Overlying unit 3 with a sharp contact was a 9-m thick, matrix-supported diamicton with abundant, angular, poorly-sorted cobbles, up to 40 cm in diameter (unit 4), and capped by loess (unit 5). The matrix-supported diamicton (unit 4) was inferred to be a deposit associated with the subsequent failure of landslide dam lake. Quartz grains from the overbank silty-sand (unit 2) returned an OSL age 16.2 ± 1.1 ka (BG 4177), which marks the culmination of fluvial aggradation at ca. 16 ka. The landslide-derived diamicton at this site and an exposure through 20 m arl terrace may be penecontemporaneous with the undated Gelongbu landslide deposit, about 1 km down river (Yin, 2014). These landslides appeared to have dammed the Yellow River forming a 30-km-long lake soon after fluvial aggradation at ca. 16 ka.

5. Discussion

5.1. Yellow River incision and tectonic uplift

The time-series of abandoned fluvial surfaces, forming terraces on 10^4 and 10^5 yr timescales, provide a measure of net incision rates for this fluvial network (Table 2) which closely reflects regional rock uplift rates (Hancock and Anderson, 2002; Pan et al., 2013). This study recognized depositional terraces with clear aggradational sequences often deposited on to bedrock lithologies of Neogene red mudstone, Eocene brick-red sandstone or granite (Fig. 7). These terrace sequences reflect multiple cycles of aggradation and degradation over the past ca. 100 ka with the record further extended to ca. 187 ka by including data from Zhao and Liu (2003) (Fig. 8; Table 2). The incision rate was calculated based on the highest elevational occurrence of fluvial deposits within terraces which was usually bar top or overbank sediments associated with aggradation, which has equivalent water levels for different basins and through time. The estimated variance for this fluvial water plane is 1–3 m based on current observations of depositional environments for the Yellow River; this datum was used to calculate apparent incision rates. Note, that the current surface elevation of terraces was not used because of added thickness between 0.5 and 15 m of overlying non-fluvial sediments. The incision rates were calculated as a least-squares linear regression with errors estimated by maximum likelihood estimation using the complete data set of terrace ages, associated elevations (Fig. 8) and for intervening intervals for the individual basins (Table 2). These rates were not calculated for the Holocene because fluvial processes were dominated by climate and human-induced changes. The incision rate for past ca. 100 ka is 1.13 ± 0.11 mm/yr (Fig. 8) with shorter intervals of time during the late Pleistocene yielding apparent incision rates between 1.4 and 0.9 mm/yr (Table 2). The incision rate for Guide Basin varies modestly between 1.3 and 1.1 mm/yr for the past 187 ka, with more variable incision rates for the Jianzha and Xunhua basins (Table 2). This variability in incision rates appears to be independent of hardness of the bedrock with mudstone occurring in both the Jianzha and the Guide basins and Granite in the Xunhua Basin, consistent with a previous study (Pan et al., 2013). The highest apparent incision rate is 1.4 mm/yr occurred in the Jianzha Basin post 11.6 ka and may reflect heightened incision after a landslide-released mega-flood at ca. 16 ka (Ma et al., 2014; Yin, 2014; Wu et al., 2016; Guo et al., 2016). In turn, the apparent incision rates were the lowest at 0.8 and 0.9 mm/yr prior to this mega-flood in the Jianzha and Xunhua basins during a period of aggradation between 25 and 15 ka (Fig. 8). The apparent incision rate is 1.13 ± 0.11 mm/yr for the past ca. 100 ka and is 0.8–1.4 mm/yr for the past ca. 20 to 15 ka across the Guide, Jianzha and Xunhua basins (Table 2). This rate of fluvial degradation is consistent with tectonic uplift rates of >0.5–2 mm/year for the late Cenozoic (Clark et al., 2005; Deng et al., 2013; Zhang and Jin, 2013; Pan et al., 2016). Thus, it appears that regional tectonic uplift was relatively consist between 1.0 and 1.5 mm/yr for past 100 ka and at yearly to multi-

Table 2
Yellow River terraces elevation, age and apparent incision rates for the Guide, Jianzha and Xunhua, basins, Yellow River, China.

Terrace number		Guide Basin			Jianzha Basin			Xunhua Basin		
		Elevation above river (m)	Terrace age (ka)	incision rate (mm/yr)	Elevation above river (m)	Terrace age (ka)	incision rate (mm/yr)	Elevation above river (m)	Terrace age (ka)	incision rate (mm/yr)
T9		252[a]	>187 ± 9.4[a]							
T8		217[a]	187 ± 9[a]	1.2						
T7		162[a]	140[a]	1.2						
T6		122[a]	105.2[a]	1.2						
		125	>37.89							
T5		102[a]	87.9[a]	1.2	95[b]	79 ± 6[b]	1.2			
T4		61[a]	52.6[a]	1.2						
		64	>30.6							
T3	a	50[a]	43.1[a]	1.2	47	65.8 ± 5.2	0.7	53	46.6 ± 3.8	1.1
		45	39.7 ± 3.4	1.1		45.9 ± 3.5	1.0			
	b				34	25.3 ± 2.4	1.3			
T2		21[a]	18.1[a]	1.2	15	17.6 ± 1.3	0.8	15	16.2 ± 1.1	0.9
16		25	19.5 ± 1.6	1.3	16	11.5 ± 0.9	1.4	21	17.2 ± 1.2	1.2
		24	20.7 ± 1.7	1.2	20	16.9 ± 1.3	1.2	20	18.5 ± 1.6	1.1
		24.5	20.5 ± 1.4	1.2						
T1		5[a]	8.6[a]							

[a] (Zhao and Liu, 2003).
[b] (Guo et al., 2016).

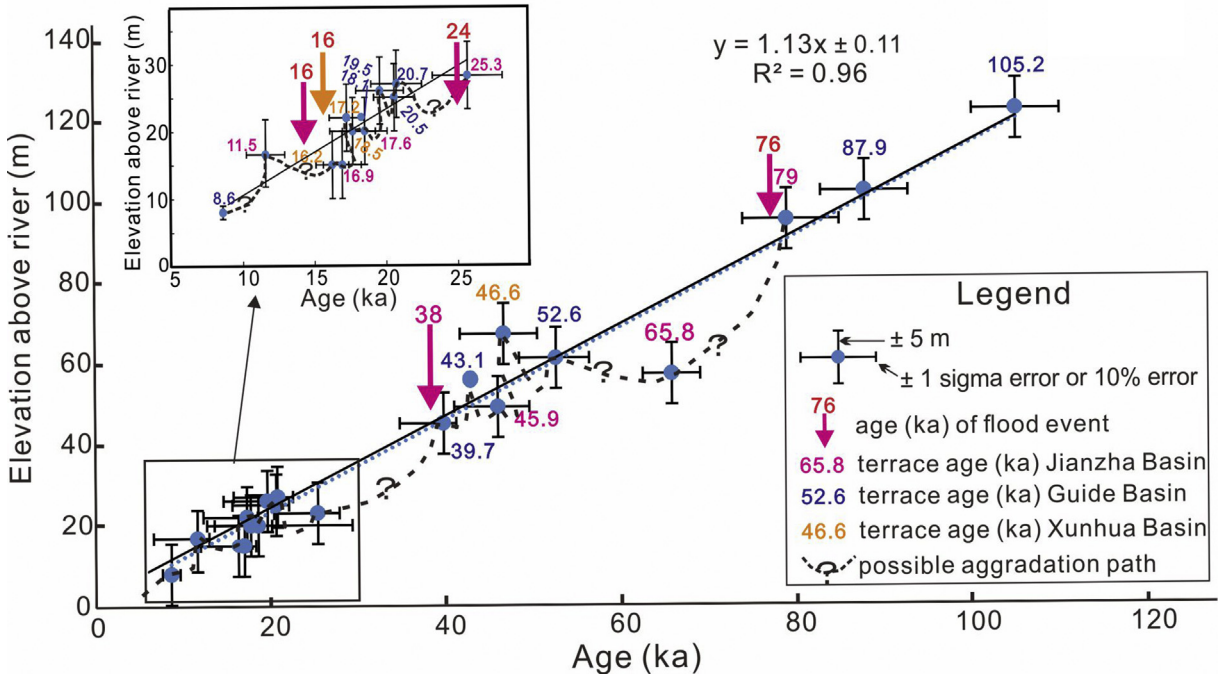

Fig. 8. Apparent river incision rate based on terrace heights and ages along the upper reaches of the Yellow River. Average apparent incision rate is 1.13 ± 0.11 mm/yr at 95% confidence interval for the past ca. 100 ka calculated by least-squares linear regression with errors by maximum likelihood estimation for the combined record from Guide, Jianzha, and Xunhua basins. The errors in OSL ages are at one sigma and for ages from Zhao and Liu (2003) a one sigma 10% error is assumed.

millennial timescales.

5.2. Terrace elevations and correlations

An inherent challenge in the correlation of fluvial terraces across basins along the Yellow River is the incompleteness of the geomorphic record. There were differential erosion and preservation of surfaces with landslides damming the main channel and tributaries, subsequent lake formation and draining (Li et al., 2011); and with variable surface elevation with subsequent loess and alluvial fan deposition. Compounding this challenge is the prior numbering of terrace surfaces from the current river, often irrespective of elevation (Li et al., 1997; Zhao and Liu, 2003; Pan et al., 2009; Hu et al., 2017). We choose to discuss the fluvial terrace record in reference to elevation for the uppermost fluvial deposit preserved within the terrace stratigraphy providing a process-linked elevation to assess aggradational and degradational associations. The terrace sequence in the Guide Basin has identified the greatest number of fluvial landforms (Zhao and Liu, 2003) compared to other nearby basins and serves as a metric to compare and to integrate terrace sequences from the Jianzha and the Xunhua basins (Table 2).

Common to many fluvial depositional systems was the preferential recognition and occurrence of the youngest landforms, with older landforms of lesser extent. This study focused on the six lowest terraces, especially those that may have been affected by penecontemporaneous landslides and subsequent failure of landslide-dammed lakes. The presented OSL ages for terrace deposits were generally consistent with previously determined TL ages (Zhao and Liu, 2003). Notable was the consistency between TL ages of ca. 18.1 and 43.1 ka for terraces at 21 and 45 m arl in the Guide Basin with corresponding OSL ages from this study of 16.9 ± 1.3, 17.2 ± 1.2 and 45.9 ± 3.5 ka (Tables 1 and 2). TL ages of 52.6 and 105.2 ka, on quartz grains from terraces at 64 and 125 m arl in Guide basin confirmed that fluvial aggradations preceded deposition of overlying alluvial fan sediments with OSL ages of 31 and 38 ka. Ultimately, we inferred that terraces at 5, 25, 45, 60, 102 and 125 m arl correspond to terraces numbered as 1, 2, 3, 4, 5, 6, with associated mean age of ca. 9, 17, 45, 52, 88 and 105 ka for three basins. Higher terraces at 162, 217 and 252 m arl may correspond to terraces 7, 8 and 9, with estimated respective ages of ca. 140, 187, and >187 ka (Table 2). There are notable exceptions, such as for a terrace at 34 m arl in Jianzha Basin which yielded an OSL age of 25.34 ± 2.44 ka (BG 4105) on quartz grains from an upper channel facies which does not conform to a numbered terrace. We recommend that terraces should be identified by elevation and age to avoid potential miss-correlations and to better understand the complex response of the Yellow River and its extensive tributary system to climatic, tectonic and intrinsic forcings.

5.3. River response to hydrologic variability during glacial and interstadial periods

In general, river incision has been attributed to a combination of three factors which for this study translates into (1) uplift of the Tibetan Plateau, (2) variable channel geometry, associated runoff and sediment yield of the Yellow River reflecting climate variability and (3) changes in base level and/or river gradient. The study area lies ~3600 km upstream of the Yellow River mouth, and it is unlikely that glacial-interglacial changes in sea level impacted incision rates (Pan et al., 2009). However, stadial to interstadial climate variability and concomitant landscape ecological responses in the catchment probably changed discharge sediment-load relations, with a net fluvial response from aggradation to degradation (Penck and Brückner, 1909; Bridgland and Westaway, 2008a; Winsemann et al., 2015).

The timing of aggradation for the last interglacial, MIS 5, remains uncertain because of the paucity luminescence ages for terraces between 100 and 130 m arl, limited to three estimates of ca. 87.9, 79.0, and 105.2 ka (Table 2; Fig. 9). This evidence indicated

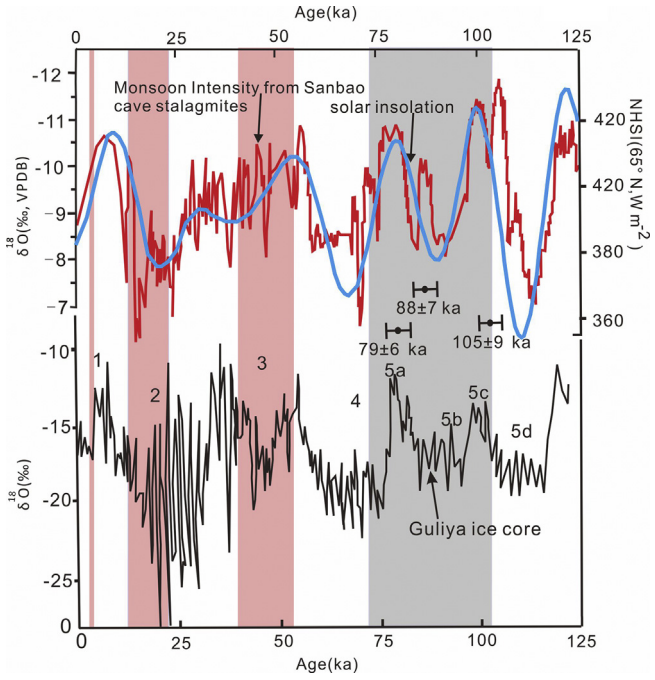

Fig. 9. Terrace aggradational phases are shown in red and gray, with the association to speleothem $\delta^{18}O$ record of Sanbao Cave (Wang et al., 2008) (red line), $\delta^{18}O$ record of the Guliya ice core (black line) (Yao et al., 1997) and summer insolation at 65° N (blue line) (Berge, 1978). Three OSL ages are the basis for inferring aggradational during MIS5. (For interpretation of the references to color in this figure legend, the reader is referred to the Web version of this article.)

sufficient sediment flux and hydrologic conditions for net aggradation, possibly associated with interstadial conditions, later in MIS 5. Equally unconstrained is state of Yellow River during the transition between MIS 5 and 4. One site in the Jianzha Basin with fluvial deposits at 52 m arl yielded a single OSL age of ca. 66 ka which indicated fluvial incision to least 10 m lower in MIS 4, than a prior terrace level (Fig. 8). This deposit yields an important elevational constraint on the degradational limit of the Yellow River and occurred after a mega-flood from a breached landslide dam in the Jianzha Basin at ca. 76 ka (Li et al., 2011; Guo et al., 2014, 2016).

The terrace sequence between 61 and 45 m arl yielded OSL ages that ranged from ca. 53 to 40 ka which reflects a prolonged period of fluvial aggradation with stadial conditions during MIS 3 (Table 2; Fig. 8). River aggradation appears to be coincident with a wetter period for the northeastern Tibetan Plateau ca. 50 to 40 ka characterized by an enhanced monsoon as inferred from $\delta^{18}O$ from speloethem records from Sanbao Cave (Wang et al., 2008) (Fig. 9), indicated by a supply-limited large set of sand dunes (Chen and Bowler, 1986; Fang, 1991; Herzschuh, 2006) and numerous high lake stands (Pachur et al., 1995; Shi et al., 1999; Shi et al., 2001; Yang et al., 2004, 2011). Monsoon intensity inferred from the Sanbao Cave $\delta^{18}O$ record appears to be positively correlated with North Hemisphere summer insolation variability at 65° N (Wang et al., 2008). A stronger Southeast Asian Monsoon in MIS 3, compared to MIS 2, may have paced fluvial aggradation (Fig. 9). These wetter conditions, with near stadial temperatures, appeared to enhanced sediment loads and foster net aggradation. This aggradational period possibly ends with a large flood emanating from Jianzha Basin at ca. 38 ka (Yin, 2014).

Another terrace aggradational complex occur between 25 and 15 m arl (Fig. 8). This complex spans from about 25 to 15 ka and formed during the last deglacial transition (Table 2) coincident with sustained melt water discharge and increasing strength of the summer monsoon (Fig. 9) (Yao et al., 1997; Liu et al., 2016). A flood at ca. 24 ka in the Jianzha Basin appears to have arrested aggradation though river level rose by 20 ka (Fig. 10). This aggradational period appears to be interrupted by a large flood sourced from Xunhua Basin ca. 16 ka (Yin, 2014).

The terrace record was fragmentary post 12 ka with a sole OSL age of 11.59 ka constraining a clear depositional terrace at 25 m arl. This terrace reflects renewed aggradation possibly with the final retreat of glaciers on the Tibetan Plateau (Wang, 1984). The lowest recognized terrace is at 5 m arl with a single OSL age of 8.6 ka on an overbank deposit (Fig. 8). Summer monsoonal precipitation for northeastern Tibetan Plateau increased in the early Holocene and reached its maximum by 8 ka (Qiu et al., 2014; Chen et al., 2016).

Stratigraphic sequences and the clustering of associated luminescence ages indicated that the upper reaches of the Yellow River may have aggraded during three broad periods in the last 100 ka; possibly late in MIS 5, between 100 and 80 ka, most of MIS 3, ca. 53–40 ka and during the last deglacial hemicycle ca. 21 to 12 ka. River aggradation appears to preferentially occur during glacial and deglacial phases with a maximum delivery of meltwater often co-occurring or subsequently with a strengthening summer monsoon as inferred from $\delta^{18}O$ record in Guliya ice core (Thompson et al., 1997; Yao et al., 1997) (Figs. 9 and 10a). A similar conclusion was inferred for a terrace sequence along Shagou River in Qilian Mountain on the northeastern Tibetan Plateau (Pan et al., 2003) and in the Lanzhou basin, ~150 km down river from Xunhua Basin (Pan et al., 2009). There appears to be equifinality on the hydrologic conditions needed to induce aggradation, associated with increased discharge, and sediment availability during glacial or glacial-interglacial transitions.

Fluvial incision at ca. 76, 38, 24 and 16 ka ago may be paced by large floods from breached landslide dams across the Yellow River that contained large lakes expanded 10s of kilometers up drainage (Yin, 2014; Guo et al., 2015, 2016) (Fig. 10b and b'). The downstream erosion associated with these large floods would also propagate up river and tributaries, as knickpoint migration until a quasi-equilibrium was reached for gradient and channel form (Qiu et al., 2014). These landslides appear to occur after peak aggradation with newly deposited valley fill against steep topography and formed dams that impounded Yellow River discharge. The landslide dams may be ephemeral, i.e. 5–25 years as indicated by a two-dimensional hydro-sedimentary model (Croissant et al., 2017), releasing flood waters and thus initiating river degradation (Fig. 10). Additional drivers of incision be may elevate discharge

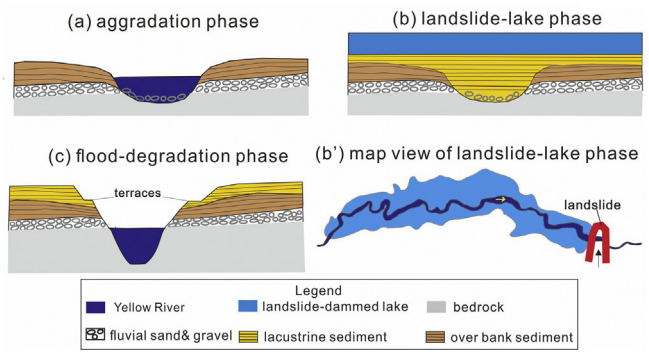

Fig. 10. Conceptual model of aggradational and degradational phases for the Yellow River in the past ca. 100 ka. (a) Aggradational phase with enhanced sediment-water delivery during stadial events at ca. 100–80 ka, 53–40 ka and 22–12 ka. (b) Shown is flooding of the Yellow River valley with landslide damming and deposition of lacustrine sediments. (b') Map view showing extent of land-slide dammed lake extending up to 70 km up stream. (c) Degradation post breach of landslide-dammed lake with large-scale flooding at 38 and 16 ka forming terraces.

with the rapid retreat of Tibetan Plateau glaciers and strengthening of the summer monsoon. Continued fluvial degradation may also reflect a shift in discharge sediment-load relations during interglacial/interstadial periods with decreased sediment production from hillslopes (Bridgland and Westaway, 2008a) (Fig. 10c).

6. Conclusions

Stratigraphic analyses with OSL dating of depositional sequences for twelve study sites within the Guide, Jianzha and Xunhua basins along an upper reach of the Yellow River identified three terrace clusters at elevations of 120 to 95 m arl, 61 to 45 m arl, and 25 to 15 m arl dated to ca. 100 to 80 ka, 53 to 40 ka, and 21 to 12 ka, respectively. Periods of river aggradation have occurred preferentially during glacial and deglacial phases with the maximum delivery of meltwater often co-occurring or subsequently with a strengthening summer monsoon. The average incision rate for this upper reach of the Yellow River for the past ca. 100 ka was 1.13 ± 0.11 mm/yr consistent with late Cenozoic uplift rates between 0.5 and 2.0 mm/yr (Clark et al., 2005; Deng et al., 2013; Zhang and Jin, 2013; Pan et al., 2016). The incision rate of this high-energy reach of the Yellow River appears to keep pace with regional tectonic uplift on 10^0–10^4 years timescales. Fluvial degradation and terrace abandonment may have been triggered by mega-floods at ca. 76, 38 and 16 ka from breached landslide dams across the Yellow River. Net downcutting of the Yellow River was possibly sustained or augmented by a shift in sediment-load discharge relations during interglacial/interstadial periods, with decreased sediment production from hillslopes (Bridgland and Westaway, 2008a). There appears to be net fluvial degradation since ca. 12 ka which may reflect an increase in effective discharge and reduced sediment supply with retreat of high altitude glaciers, increasing strength of the summer monsoon and anthropogenic effects in the late Holocene.

Acknowledgements

This work was supported by an award from the Chinese Scholarship Council (201506560011) to X.G. and funding from Geoluminescence Dating Research Laboratory at Baylor University, USA, Natural Science Foundation of Shandong Province, China (ZR2015JL015), and Chinese NSFC (41462006, 41672167 and 41761144073). The comments and discussions with Shengli Yang and Yougui Song are much appreciated; we are grateful for statistical assistance provided by Peng Liang. The comments of two reviewers and the editor were helpful in refining the presentation; and their forbearance is much appreciated.

Appendix A. Supplementary data

Supplementary data related to this article can be found at https://doi.org/10.1016/j.quascirev.2018.07.005.

References

Antoine, P., Lautridou, J.P., Laurent, M., 2000. Long-term fluvial archives in NW France: response of the Seine and Somme rivers to tectonic movements, climatic variations and sea-level changes. Geomorphology 33, 183–207.
Bøtter, J.,L., Bulur, E., Duller, G., Murray, A., 2000. Advances in luminescence instrument systems. Radiat. Meas. 32, 523–528.
Bridgland, D., 2000. River terrace systems in north-west Europe: an archive of environmental change, uplift and early human occupation. Quat. Sci. Rev. 19, 1293–1303.
Bridgland, D.R., Westaway, R., 2008a. Climatically controlled river terrace staircases: a worldwide Quaternary phenomenon. Geomorphology 98, 285–315.
Bridgland, D.R., Westaway, R., 2008b. Preservation patterns of Late Cenozoic fluvial deposits and their implications: results from IGCP 449. Quat. Int. 189, 5–38.
Bridgland, D.R., Demir, T., Seyrek, A., Daoud, M., Romieh, M.A., Westaway, R., 2017. River terrace development in the NE Mediterranean region (Syria and Turkey): patterns in relation to crustal type. Quat. Sci. Rev. 166, 307–323.
Bull, W.B., 1990. Stream-terrace genesis: implications for soil development. Geomorphology 3, 351–367.
Chen, K., Bowler, J., 1986. Late Pleistocene evolution of salt lakes in the Qaidam basin, Qinghai province, China. Palaeogeogr. Palaeoclimatol. Palaeoecol. 54, 87–104.
Chen, F., Wu, D., Chen, J., Zhou, A., Yu, J., Shen, J., Wang, S., Huang, X., 2016. Holocene moisture and East Asian summer monsoon evolution in the northeastern Tibetan Plateau recorded by Lake Qinghai and its environs: a review of conflicting proxies. Quat. Sci. Rev. 154, 111–129.
Church, M., Ryder, J.M., 1972. Paraglacial sedimentation: a consideration of fluvial processes conditioned by glaciation. Geol. Soc. Am. Bull. 83, 3059–3072.
Clark, M.K., House, M.A., Royden, L.H., Whipple, K.X., Burchfiel, B.C., Zhang, X., Tang, W., 2005. Late cenozoic uplift of southeastern Tibet. Geology 33, 525–528.
Cordier, S., Adamson, K., Delmas, M., Calvet, M., Harmand, D., 2017. Of ice and water: quaternary fluvial response to glacial forcing. Quat. Sci. Rev. 166, 57–73.
Craddock, W.H., Kirby, E., Harkins, N.W., Zhang, H., Shi, X., Liu, J., 2010. Rapid fluvial incision along the Yellow River during headward basin integration. Nat. Geosci. 3, 209–213.
Croissant, T., Lague, D., Steer, P., Davy, P., 2017. Rapid post-seismic landslide evacuation boosted by dynamic river width. Nat. Geosci. 10, 680–684.
Deng, B., Liu, S.G., Li, Z.W., Jansa, L.F., Liu, S., Wang, G.Z., Sun, W., 2013. Differential exhumation at eastern margin of the Tibetan Plateau, from apatite fission-track thermochronology. Tectonophysics 591, 98–115.
Durcan, J.A., Duller, G.A., 2011. The fast ratio: a rapid measure for testing the dominance of the fast component in the initial OSL signal from quartz. Radiat. Meas. 46, 1065–1072.
Egholm, D.L., Knudsen, M.F., Sandiford, M., 2013. Lifespan of mountain ranges scaled by feedbacks between landsliding and erosion by rivers. Nature 498, 475–478.
Fain, J., Soumana, S., Montret, M., Miallier, D., Pilleyre, T., Sanzelle, S., 1999. Luminescence and ESR dating Beta-dose attenuation for various grain shapes calculated by a Monte-Carlo method. Quat. Geochronol. 18, 231–234.
Fang, J.Q., 1991. Lake evolution during the past 30,000 years in China, and its implications for environmental change. Quat. Res. 36, 37–60.
Fang, X., Yan, M., Van der Voo, R., Rea, D.K., Song, C., Parés, J.M., Gao, J., Nie, J., Dai, S., 2005. Late cenozoic deformation and uplift of the NE Tibetan plateau: evidence from high-resolution magnetostratigraphy of the Guide basin, Qinghai province, China. Geol. Soc. Am. Bull. 117, 1208–1225.
Galbraith, R.F., Roberts, R.G., 2012. Statistical aspects of equivalent dose and error calculation and display in OSL dating: an overview and some recommendations. Quat. Geochronol. 11, 1–27.
Galbraith, R.F., Roberts, R.G., Laslett, G.M., Yoshida, H., Olley, J.M., 1999. Optical dating of single and multiple grains of quartz from Jinmium rock shelter, northern Australia: Part I, experimental design and statistical models. Archaeometry 41, 339–364.
Guo, X.H., 2017. Relationship between landslide-dammed lakes with the evolution of upper stream of the Yellow River from Longyang Gorge to Liujia Gorge on northeast margin of Tibet Plateau. Chang'an University, Xi'an (A Ph.D. dissertation in Chinese with English abstract).
Guo, Z., Fedoroff, N., An, Z., 1991. Genetic Types of the Holocene Soil and the Pleistocene Paleosols in the Xifeng Loess Section in central China. Loess, Enviro. Glob. Chang. Science Press, Beijing, pp. 93–111.
Guo, Y.J., Zhang, J.F., Qiu, W.L., Hu, G., Zhuang, M.G., Zhou, L.P., 2012. Luminescence dating of the Yellow River terraces in the Hukou area, China. Quat. Geochronol. 10, 129–135.
Guo, X.H., Lai, Z.P., Sun, Z., Li, X.L., Yang, T.B., 2014. Luminescence dating of Suozi landslide in the upper Yellow River of the Qinghai-Tibetan plateau, China. Quat. Int. 349, 159–166.
Guo, X.H., Lai, Z.P., Lu, Y.D., Li, X.L., Sun, Z., 2015. Optically stimulated luminescence (OSL) chronology of the Dehenglong landslide from Longyang gorge to Liujia gorge along upper Yellow River, China. Acta Geol. Sin-Engl 1, 242–250.
Guo, X.H., Sun, Z., Lai, Z.P., Lu, Y.D., Li, X.L., 2016. Optical dating of landslide-dammed lake deposits in the upper Yellow River, Qinghai-Tibetan Plateau, China. Quat. Int. 392, 233–238.
Hancock, G.S., Anderson, R.S., 2002. Numerical modeling of fluvial strath-terrace formation in response to oscillating climate. Geol. Soc. Am. Bull. 114, 1131–1142.
Harkins, N., Kirby, E., Heimsath, A., Robinson, R., Reiser, U., 2007. Transient fluvial incision in the headwaters of the Yellow River, northeastern Tibet, China. J. Geophys. Res.: Earth Surface 112. https://doi.org/10.1029/2006JF000570. F03S04.
He, Z., Zhang, X., Bao, S., Qiao, Y., Sheng, Y., Liu, X., He, X., Yang, X., Zhao, J., Liu, R., 2015. Multiple climatic cycles imprinted on regional uplift-controlled fluvial terraces in the lower Yalong River and Anning River, SE Tibetan Plateau. Geomorphology 250, 95–112.
Herzschuh, U., 2006. Palaeo-moisture evolution in monsoonal Central Asia during the last 50,000 years. Quat. Sci. Rev. 25, 163–178.
Hou, G., Lai, Z., Sun, Y., Ye, M., 2012. Luminescence and radiocarbon chronologies for the xindian culture site of Lamafeng in the guanting basin on the NE edge of the Tibetan plateau. Quat. Geochronol. 10, 394–398.
Hu, Z., Pan, B., Guo, L., Vandenberghe, J., Liu, X., Wang, J., Fan, Y., Mao, J., Gao, H., Hu, X., 2016. Rapid fluvial incision and headward erosion by the Yellow River along the Jinshaan gorge during the past 1.2 Ma as a result of tectonic extension. Quat. Sci. Rev. 133, 1–14.
Hu, Z., Pan, B., Bridgland, D., Vandenberghe, J., Guo, L., Fan, Y., Westaway, R., 2017.

The linking of the upper-middle and lower reaches of the Yellow River as a result of fluvial entrenchment. Quat. Sci. Rev. 166, 324–338.
Korup, O., Montgomery, D.R., 2008. Tibetan plateau river incision inhibited by glacial stabilization of the Tsangpo gorge. Nature 455, 786–789.
Korup, O., Densmore, A.L., Schlunegger, F., 2010. The role of landslides in mountain range evolution. Geomorphology 120, 77–90.
Li, J., 1991. The environmental effects of the uplift of the Qinghai-Xizang Plateau. Quat. Sci. Rev. 10, 479–483.
Li, J., Fang, X., Ma, H., Zhu, J., Pan, B., Chen, H., 1996. Geomorphological and environmental evolution in the upper reaches of the Yellow River during the late Cenozoic. Sci. China Earth Sci. 39, 380–390.
Li, J., Fang, X., Van der Voo, R., Zhu, J., Niocaill, C.M., Ono, Y., Pan, B., Zhong, W., Wang, J., Sasaki, T., 1997. Magnetostratigraphic dating of river terraces: rapid and intermittent incision by the Yellow River of the northeastern margin of the Tibetan Plateau during the Quaternary. J. Geophys. Res.: Solid Earth 102, 10121–10132.
Li, X., Guo, X., Li, W., 2011. Mechanism of giant landslides from Longyangxia valley to Liujiaxia valley along upper Yellow River. J. Eng. Geol. 19, 516–529 (In Chinese with English abstract).
Li, W., Dong, Y.P., Guo, A.L., Liu, X.M., Zhou, D.W., 2013. Chronology and tectonic significance of cenozoic faults in the Liupanshan arcuate tectonic belt at the northeastern margin of the qinghai-Tibet plateau. J. Asian Earth Sci. 73, 103–113.
Limaye, A., Lamb, M.P., 2016. Numerical model predictions of autogenic fluvial terraces and comparison to climate change expectations. J. Geophys. Res.: Earth Surface 121, 512–544.
Liu, T., 1985. Loess and the Environment. China Ocean Press, Beijing, pp. 230–251.
Liu, X.J., Madsen, D.B., Liu, R., Sun, Y., Wang, Y., 2016. Holocene lake level variations of Longmu Co, western Qinghai-Tibetan Plateau. Environ. Earth Sci. 75, 1–14.
Ma, M., Dong, G., Chen, F., Meng, X., Wang, Z., Elston, R., Li, G., 2014. Process of paleofloods in Guanting basin, Qinghai Province, China and possible relation to monsoon strength during the mid-Holocene. Quat. Int. 321, 88–96.
Mejdahl, V., Christiansen, H.H., 1994. Procedures used for luminescence dating of sediments. Quat. Sci. Rev. 13, 403–406.
Miao, Q., Qian, F., Zhao, Z., Liu, X., 2012. Terraces and evolution of the Yellow River in the Guide segment. Geol. Surv. Res. 35, 34–38 in Chinese with English abstract).
Molnar, P., Brown, E.T., Burchfiel, B.C., Deng, Q., Feng, X., Li, J., Raisbeck, G.M., Shi, J., Zhangming, W., Yiou, F., 1994. Quaternary climate change and the formation of river terraces across growing anticlines on the north flank of the Tien Shan, China. J. Geol. 102, 583–602.
Murray, A.S., Wintle, A.G., 2003. The single aliquot regenerative dose protocol: potential for improvements in reliability. Radiat. Meas. 37, 377–381.
Nivière, B., Lacan, P., Regard, V., Delmas, M., Calvet, M., Huyghe, D., Roddaz, B., 2016. Evolution of the late Pleistocene aspe river (western pyrenees, France). Signature of climatic events and active tectonics. Compt. Rendus Geosci. 348, 203–212.
Pachur, H.J., Wünnemann, B., Zhang, H., 1995. Lake evolution in the Tengger desert, northwestern China, during the last 40,000 years. Quat. Res. 44, 171–180.
Pan, B.T., Li, J.J., Cao, J., Chen, F., 1996. Study on the geomorphic evolution and development of the Yellow River in the Hualong basin. Mt. Res. 14, 153–158 (In Chinese with English abstract).
Pan, B.T., Burbank, D., Wang, Y.X., Wu, G.J., Li, J.J., Guan, Q.Y., 2003. A 900 k.y. record of strath terrace formation during glacial-interglacial transitions in northwest China. Geology 31, 957–960.
Pan, B.T., Su, H., Hu, Z.B., Hu, X.F., Gao, H.S., Li, J.J., Kirby, E., 2009. Evaluating the role of climate and tectonics during non-steady incision of the Yellow River: evidence from a 1.24 Ma terrace record near Lanzhou, China. Quat. Sci. Rev. 28, 3281–3290.
Pan, B., Hu, X., Gao, H., Hu, Z., Cao, B., Geng, H., Li, Q., 2013. Late Quaternary river incision rates and rock uplift pattern of the eastern Qilian Shan Mountain, China. Geomorphology 184 (2013), 84–97.
Pan, Y.J., Shen, W.B., Hwang, C.W., Liao, C.M., Zhang, T.X., Zhang, G.Q., 2016. Seasonal mass changes and crustal vertical deformations constrained by GPS and GRACE in the Northeastern Tibet. Sensors 16, 1211. https://doi.org/10.3390/s16081211.
Penck, A., Brückner, E., 1909. Die alpen im Eiszeitalter. Tauchnitz Leipzig (in German).
Prescott, J.R., Hutton, J.T., 1994. Cosmic ray contributions to dose rates for luminescence and ESR dating: large depths and long-term time variations. Radiat. Meas. 23, 497–500.
Qinghai Earthquake Administration, 1989. Report on Validation for Basically Seismic Intensity and Risk for Engineering Earthquakes in Lijia Power Station along Yellow River: Xining (in Chinese).
Qinghai Geological Survey, 1971. Regional Geological Investigation for 1:200,000 Scale (In Chinese).
Qiu, W.L., Zhang, J.F., Wang, X.Y., Guo, Y.J., Zhuang, M.G., Fu, X., Zhou, L.P., 2014. The evolution of the shiwanghe River valley in response to the Yellow River incision in the Hukou area, shaanxi, China. Geomorphology 215, 34–44.
Shi, Y., Liu, X., Li, B., Yao, T., 1999. A very strong summer monsoon event during 30–40 ka BP in the Qinghai-Xizang (Tibet) Plateau and its relation to precessional cycle. Chin. Sci. Bull. 44, 1851–1858.
Shi, Y., Yu, G., Liu, X., Li, B., Yao, T., 2001. Reconstruction of the 30-40 ka BP enhanced Indian monsoon climate based on geological records from the Tibetan Plateau. Palaeogeogr. Palaeoclimatol. Palaeoecol. 169, 69–83.
Rittenour, T.M., 2008. Luminescence dating of fluvial deposits: applications to geomorphic, palaeoseismic and archaeological research. Boreas 37, 613–635.
Schokker, J., Cleveringa, P., Murray, A.S., Wallinga, J., Westerhoff, W.E., 2005. An OSL dated middle and late quaternary sedimentary record in the Roer Valley Graben (southeastern Netherlands). Quat. Sci. Rev. 24, 2243–2264.
Thompson, L.O., Yao, T., Davis, M., Henderson, K., Mosley-Thompson, E., Lin, P.N., Beer, J., Synal, H.A., ColeDai, J., Bolzan, J., 1997. Tropical climate instability: the last glacial cycle from a Qinghai-Tibetan ice core. Science 276, 1821–1825.
Vandenberghe, J., 2003. Climate forcing of fluvial system development: an evolution of ideas. Quat. Sci. Rev. 22, 2053–2060.
Vandenberghe, J., 2008. The fluvial cycle at cold-warm-cold transitions in lowland regions: a refinement of theory. Geomorphology 98, 275–284.
Wang, Z., 1984. A Preliminary research on the ancient glacial relics in the Mt. Namjagbarwa region. J. Mt. Res. 3, 1–11 in Chinese with English abstract).
Wang, Y.J., Cheng, H., Edwards, R.L., Kong, X.G., Shao, X.H., Chen, S.T., Wu, J.Y., Jiang, X.Y., An, Z.S., 2008. Millennial and orbital scale changes in the East Asian monsoon over the past 224,000 years. Nature 451, 1090–1093.
Wang, P., Jiang, H.C., Yuan, D.Y., Liu, X.W., Zhang, B., 2010. Optically stimulated luminescence dating of sediments from the Yellow River terraces in Lanzhou: tectonic and climatic implications. Quat. Geochronol. 5, 181–186.
Westaway, R., Bridgland, D.R., 2014. Relation between alternations of uplift and subsidence revealed by Late Cenozoic fluvial sequences and physical properties of the continental crust. Boreas 43, 505–527.
Westaway, R., Bridgland, D., Mishra, S., 2003. Rheological differences between Archaean and younger crust can determine rates of Quaternary vertical motions revealed by fluvial geomorphology. Terra. Nova 15, 287–298.
Winsemann, J., Lang, J., Roskosch, J., Polom, U., Böhner, U., Brandes, C., Glotzbach, C., Frechen, M., 2015. Terrace styles and timing of terrace formation in the Weser and Leine valleys, northern Germany: response of a fluvial system to climate change and glaciation. Quat. Sci. Rev. 123, 31–57.
Wintle, A.G., Murray, A.S., 2006. A review of quartz optically stimulated luminescence characteristics and their relevance in single-aliquot regeneration dating protocols. Radiat. Meas. 41, 369–391.
Wu, Q., Zhao, Z., Liu, L., Granger, D.E., Wang, H., Cohen, D.J., Wu, X., Ye, M., Bar-Yosef, O., Lu, B., 2016. Outburst flood at 1920 BCE supports historicity of China's Great Flood and the Xia dynasty. Science 353, 579–582.
Yang, B., Shi, Y., Braeuning, A., Wang, J., 2004. Evidence for a warm-humid climate in arid northwestern China during 40-30 ka BP. Quat. Sci. Rev. 23, 2537–2548.
Yang, X., Scuderi, L., Paillou, P., Liu, Z., Li, H., Ren, X., 2011. Quaternary environmental changes in the drylands of China-a critical review. Quat. Sci. Rev. 30, 3219–3233.
Yao, T., Thompson, L., Shi, Y., Jiao, K., Zhang, X., 1997. A study on the climate changes from Guliya ice core records since last interglacial period. Sci. China, Ser. A D. 6, 447–452.
Yin, Z., 2014. The Spatial and Temporal Distribution, Evolution Process and Key Triggering Factors of Super Large-scale Landslides in the Middle Upper Reaches of Yellow River. University of Chinese Academy of Sciences, Beijing. A Ph.D. dissertation in Chinese with English abstract).
Zhang, T.Y., Jin, S.G., 2013. Estimate of glacial isostatic adjustment uplift rate in the Tibetan Plateau from Grace and GIA models. J. Geodyn. 72, 59–66.
Zhang, X., Yang, S., Guo, X., 2007. Study on Plate Tectonics in Qinghai Province. Geological Publishing House, Beijing.
Zhang, J.F., Qiu, W.L., Li, R.Q., Zhou, L.P., 2009. The evolution of a terrace sequence along the Yellow River (HuangHe) in Hequ, Shanxi, China, as inferred from optical dating. Geomorphology 109, 54–65.
Zhang, H.P., Zhang, P.Z., Champagnac, J.D., Molnar, P., Anderson, R.S., Kirby, E., Craddock, W.H., Liu, S.F., 2014. Pleistocene drainage reorganization driven by the isostatic response to deep incision into the northeastern Tibetan Plateau. Geology 42, 303–306.
Zhao, Z.M., Liu, B.C., 2003. Relation between the formation of the Yellow River valley landforms from Gonghe, Qinghai to Lanzhou, gansu and the uplift in northeast part of qinghai-xizang plateau. Northwest. Geol. 36, 1–12 (In Chinese with English abstract).
Zhou, B., 2011. Research on Development Characteristic and Mass Mechanism of Super Large Landslide in the Upper Yellow River. Chang'an University, Xi'an. A Ph.D. dissertation in Chinese with English abstract).